# A NOVEL ITERATIVE CALIBRATION APPROACH FOR THERMAL INFRARED CAMERAS

*Andreas Ellmauthaler*[1]*, Eduardo A. B. da Silva*[1]*, Carla L. Pagliari*[2]*, Jonathan N. Gois*[1]
*and Sergio R. Neves*[3]

[1] Universidade Federal do Rio de Janeiro, PEE/COPPE/DEL, Rio de Janeiro, Brazil
[2] Instituto Militar de Engenharia, Department of Electrical Engineering, Rio de Janeiro, Brazil
[3] Instituto de Pesquisas da Marinha, Rio de Janeiro, Brazil

## ABSTRACT

The accurate geometric calibration of thermal infrared (IR) cameras is of vital importance in many computer vision applications. In general, the calibration procedure consists of localizing a set of calibration points within a calibration image. This set is subsequently used to solve for the camera parameters. However, due to the physical limitations of the IR acquisition process, the localization of the calibration points often poses difficulties, subsequently leading to unsatisfying calibration results. In this work a novel IR camera calibration approach is introduced. It is able to localize the calibration points within the images of a conventional calibration board consisting of miniature light-bulbs with improved accuracy. Our algorithm models the radiation pattern of each light bulb as an ellipse and considers the center of mass of the extracted ellipsoidal region as the starting calibration point, which is refined iteratively using alternating mappings to and from an undistorted grid model. The proposed processing chain leads to a significantly reduced calibration error when compared to the state-of-the-art. Furthermore, the proposed methodology can also be used to calibrate visible-light cameras thus being suitable for the calibration of multiple camera rigs involving both visible-light and IR cameras.

***Index Terms—*** camera calibration, infrared imaging, iterative, ellipse fitting

## 1. INTRODUCTION

Camera calibration is the preliminary step in many computer vision applications such as 3D reconstruction, robot navigation or image registration. Generally speaking, it refers to the process of finding the set of calibration parameters which allow us to map a 3D scene onto a 2D image plane. The sought parameters include the optical properties of the camera (intrinsic parameters), such as its center and focal length, as well as the relative position of the camera with respect to some object of interest (extrinsic parameters).

The most popular calibration techniques usually require the camera to take several images of a planar calibration device, located at least at two different orientations [1, 2, 3]. The actual calibration procedure then tries to localize a set of points within the calibration pattern of each view and computes the camera parameters based on these extracted calibration points. Typical choices of calibration points include the corners of a square pattern (checkerboard), the centers of circles, or the centers of ring patterns [2].

Whereas the current state-of-the-art allows a remarkable precision for the calibration of visible-light cameras, results are still far from optimal for thermal infrared (IR) cameras. In fact, the mean reprojection error (MRE) - defined as the average position error when mapping the calibration point positions from the world coordinate system to the image plane using the computed calibration parameters - usually differs by a power of 10 between the calibration results of visible-light (MRE in the order of $10^{-2}$ [2, 3]) and IR cameras (MRE in the order of $10^{-1}$ [4, 5, 6]). The reason behind this is twofold. In the first place, the construction of a calibration device which allows for the exact localization of the calibration points within the IR image is usually a cumbersome task. Secondly, only a few studies have focused on the geometric calibration of IR cameras [5, 7].

In this paper a new approach to thermal IR camera calibration is introduced which significantly improves on the calibration results of existing methods. It utilizes a novel iterative calibration point localization scheme, based on the calculation of the center of mass of ellipsoidal regions. Note that the proposed system can also be used for the calibration of visible-light cameras and is thus suitable for the calibration of multiple camera rigs involving combinations of thermal IR and visible-light cameras. Such multiple camera setups may be used for tasks such as image fusion [8, 9] and autonomous driving [4], and represent an interesting platform for new computer vision applications.

The structure of this paper is as follows: The necessary background on the theory of camera calibration is presented in Section 2. Section 3 starts with an analysis of the state-of-the-art of IR camera calibration before introducing the proposed camera calibration scheme in detail. Section 4 discusses the obtained results and compares them with other state-of-the-art IR camera calibration schemes. Finally, our conclusions are given in Section 5.

## 2. BACKGROUND

We start our discussion with the basic pinhole camera model which is used in most computer vision applications to transform 3D world coordinates to 2D image coordinates. Let an image point in 2D be represented by the homogeneous vector $\mathbf{x} = [x\ y\ 1]^T$ and its counterpart in the 3D world coordinate system by the homogeneous vector $\mathbf{X} = [X\ Y\ Z\ 1]^T$. The general mapping given by the pinhole camera can then be expressed by [10]

$$\mu\mathbf{x} = \mathbf{K}\,[\mathbf{R}\,\mathbf{t}]\,\mathbf{X}\,, \quad \text{with } \mathbf{K} = \begin{bmatrix} \alpha_x & s & x_0 \\ 0 & \alpha_y & y_0 \\ 0 & 0 & 1 \end{bmatrix}\,, \qquad (1)$$

where $\mu$ is an arbitrary scale factor, $\mathbf{R}$ and $\mathbf{t}$ are the extrinsic camera parameters and $\mathbf{K}$ is called the camera intrinsic matrix [1] or camera calibration matrix [10]. The parameters of the $3 \times 3$ rotation matrix $\mathbf{R}$ and the $3 \times 1$ translation vector $\mathbf{t}$ represent the placement of the world coordinate system with respect to the camera coordinate system whereas $\mathbf{K}$ contains the internal camera parameters in terms of pixel dimensions. These are the focal length $(\alpha_x, \alpha_y)$ and the principal point $(x_0, y_0)$ of the camera in the $x$ and $y$ direction respectively,

The authors would like to thank the Brazilian Funding Agencies CAPES/Pro-Defesa and CNPq for their financial support.

as well as the parameter $s$ which describes the skewness of the two image axes.

When using a planar calibration device we can assume without loss of generality that the calibration pattern is located on the plane $Z = 0$ in the world coordinate system. Thus, we can rewrite eq. (1) such that

$$\mu \begin{bmatrix} x \\ y \\ 1 \end{bmatrix} = \mathbf{K} \begin{bmatrix} \mathbf{r_1} & \mathbf{r_2} & \mathbf{r_3} & \mathbf{t} \end{bmatrix} \begin{bmatrix} X \\ Y \\ 0 \\ 1 \end{bmatrix} = \mathbf{K} \begin{bmatrix} \mathbf{r_1} & \mathbf{r_2} & \mathbf{t} \end{bmatrix} \begin{bmatrix} X \\ Y \\ 1 \end{bmatrix} = \mathbf{H}\bar{\mathbf{X}} \,, \quad (2)$$

where $\mathbf{R}$ is given by $[\mathbf{r_1}\ \mathbf{r_2}\ \mathbf{r_3}]$, $\mathbf{H} = \mathbf{K}\,[\mathbf{r_1}\ \mathbf{r_2}\ \mathbf{t}]$ is called a homography matrix and $\bar{\mathbf{X}} = [X\ Y\ 1]^T$. Please note that the $3 \times 3$ matrix $\mathbf{H}$ is only defined up to a scale factor.

As was shown in [1], a first estimate of the intrinsic and extrinsic parameters can be obtained by knowing the homographies $\mathbf{H}$ between the calibration pattern and its image for two or more views. These homographies can be obtained by applying a closed-form algorithm such as the Direct Linear Transformation (DLT) algorithm in combination with a nonlinear minimization of the reprojection error using e.g. the iterative Levenberg-Marquardt algorithm [10].

However, this first estimate of the calibration parameters is not optimal since a) it is obtained by applying the singular value decomposition which minimizes an algebraic distance that is not physically meaningful, and b) does not incorporate radial and tangential distortion arising from the optical lens employed in the camera. The radial and tangential distortion can be approximated using the following expression [11, 12]

$$\mathcal{F}_{\mathcal{D}}\left(\mathbf{x}_d, k, p\right) = \begin{bmatrix} x_d\left(k_1 r^2 + k_2 r^4 + \ldots\right) + \left(2p_1 x_d y_d + p_2(r^2 + 2x_d^2)\right) \\ y_d\left(k_1 r^2 + k_2 r^4 + \ldots\right) + \left(p_1(r^2 + 2y_d^2) + 2p_2 x_d y_d\right) \end{bmatrix}, \quad (3)$$

where $\mathbf{x}_d = [x_d\ y_d]^T$ are the distorted, normalized image coordinates, $k = \{k_1, k_2, \ldots\}$ and $p = \{p_1, p_2\}$ are the coefficients of the radial and tangential distortion, respectively, and $r = \sqrt{x_d^2 + y_d^2}$. Thus, the previously obtained calibration parameters are merely used as the initial guess in a final global optimization step which estimates the complete set of parameters by applying a geometrically meaningful distance measure. This optimization is done by iteratively minimizing the following functional [1]

$$\sum_i \sum_j \left\| \mathbf{x}'_{ij} - \breve{\mathbf{x}}\left(\mathbf{K}, k, p, \mathbf{R}_i, \mathbf{t}_i, \bar{\mathbf{X}}'_j\right) \right\|^2 , \quad (4)$$

where $\mathbf{x}'_{ij}$ is the sub-pixel position of the $j^{\text{th}}$ calibration point in the $i^{\text{th}}$ calibration image, and $\breve{\mathbf{x}}\left(\mathbf{K}, k, p, \mathbf{R}_i, \mathbf{t}_i, \bar{\mathbf{X}}'_j\right)$ is the projection of the corresponding calibration point $\bar{\mathbf{X}}'_j$ from the 3D world coordinate system.

Given the calibration point positions in the real world and camera coordinate system, various off-the-shelf solutions for camera calibration exist. Among them, the *OpenCV Camera Calibration Toolbox* [13] as well as the *Camera Calibration Toolbox for Matlab* [14] are predominately used.

## 3. PROPOSED ALGORITHM

An IR image is the result of the acquisition of thermal radiation of a scene, producing a 2D map that depends on the temperature, emissivity and reflexivity variations of the respective scene [8]. Consequently, existing camera calibration approaches based on black/white calibration patterns cannot be employed for IR camera calibration straightforwardly since such calibration devices do not appear in the IR image in most cases.

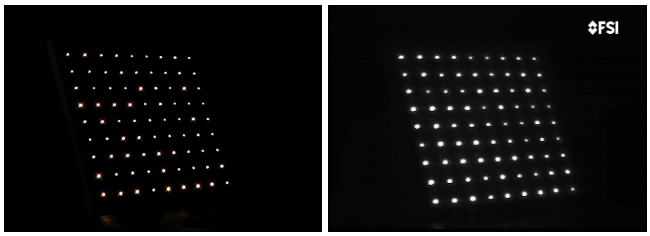


**Fig. 1:** *Calibration device consisting of 81 light bulbs, arranged in a* $9 \times 9$ *matrix, in the visible-light (left) and IR spectrum (right).*

Given this fact, a number of approaches have been proposed for IR camera calibration. For instance, Prakash et al. [15] advocate the use of a heated chessboard as an appropriate calibration device. They argue that due to the different IR emissivity of black and white regions, it is possible to extract the corner points of the chessboard pattern in the IR modality and use these points for calibration purposes. However, as reported in [6], in general such an IR calibration image fails to exhibit crisp corners, consequently preventing the precise localization of these corner points in the IR image. Thus, they suggest a different calibration pattern which consists of a grid of regularly sized squares, cut out of a material that is opaque in the IR modality. The authors demonstrate that when held in front of a backdrop with a different temperature than the ambiance, such a pattern can be identified in the IR domain and allows for a more reliable extraction of the corner points. Another interesting strategy is chosen in [4], where a planar black/white checkerboard pattern, augmented by a set of resistors mounted in the centroid of each square, is used as a calibration device. In this approach, the corners of the black/white squares are utilized for the calibration of a visible-light camera, whereas the energized resistors are used for IR camera calibration.

The most popular IR camera calibration pattern involves the use of miniature light bulbs, equidistantly mounted on a planar calibration board [5, 7]. This configuration is of special interest since, when turned on, heat and light are simultaneously emitted by the light bulbs causing the calibration pattern to appear in both the visible-light and IR spectrum. This is demonstrated in Fig. 1, where a calibration device consisting of 81 light bulbs, arranged in a $9 \times 9$ matrix, is depicted in the visible-light and IR spectrum.

Whereas many improvements have been achieved in recent years to optimize visible-light camera calibration, state-of-the-art IR camera calibration methods still lack in precision. This is mainly due to the physical properties of IR sensors. In more detail, images obtained from an IR sensor tend to have a low signal-to-noise ratio and fail to exhibit sharp transitions between objects of different temperature, hence considerably complicating the exact localization of the calibration points [16].

In this work a new approach for the calibration of thermal IR cameras is proposed. Our method is able to overcome the drawbacks of traditional approaches by using a novel processing chain which iteratively refines the positions of the calibration points, yielding more accurate estimates of the camera calibration parameters. The complete algorithm can be found in Fig. 2. In the remainder of this section the individual steps will now be explained in detail.

### 3.1. Calibration point localization

Given $N$ rotated and translated views of the calibration device depicted in Fig. 1, our algorithm starts off by extracting the exact subpixel positions of the calibration points in each calibration image.

**Objective**

Given $N$ rotated views of the calibration device of Fig. 1, calculate the IR camera parameters.

**Algorithm**

1) For each calibration image **find the sub-pixel positions of the calibration points**:
   - Perform **gray-scale thresholding** to separate the light bulb regions from the background.
   - **Fit an ellipse** to each extracted light bulb region.
   - **Compute the center of mass** of each ellipsoidal region within the calibration image.
   - Use the DLT algorithm in conjunction with the computed centers of mass to **determine a first estimate of the homography matrix H**.
   - **Refine the calculated homography** by minimizing the cost function of eq. (5).
   - **Compute the final calibration point positions** by applying the refined homography to the calibration point positions in the world coordinate system.
2) Use the calibration point positions of 1) to **estimate the IR camera parameters**.
3) **Iteratively refine the calibration point positions** until convergence:
   - **Remove optical distortions and map the calibration images onto a fronto-parallel plane** using the previously calculated camera parameters.
   - **Repeat 1)** for all calibration images in the fronto-parallel plane.
   - **Remap the new calibration points** back onto the original image plane.
   - **Re-estimate the IR camera parameters** as in 2).

**Fig. 2:** *Proposed IR camera calibration algorithm.*

For this purpose we first binarize the calibration images using the adaptive thresholding scheme of [3], separating the light bulb regions from the background. The result of the thresholding operation, employed on the IR calibration image of Fig. 1 is shown in the left-hand side of Fig. 3. Please note that the wrongly extracted regions belonging to the watermark in the upper right corner of the IR calibration images (see Fig. 1) were excluded using a simple $k$-means clustering operation [17].

After the thresholding operation, the extracted light bulb regions may appear with irregular shapes in the binarized image and may no longer resemble the expected ellipsoidal radiation pattern. Thus, as a second step, the extracted light bulb regions need to be further processed. This is accomplished by fitting an ellipse to the boundary pixels of each region and by subsequently using the area of the computed ellipse as the new light bulb region. In our implementation we utilize the Canny edge detector [18] to compute the region boundaries. The ellipse fitting is performed by employing the algorithm of [19] which calculates the ellipses using a least-squares-based algorithm. The right-hand side of Fig. 3 shows the extracted ellipse for a single light bulb region from the IR calibration image of Fig. 1.

A first estimate of the calibration point positions is obtained by calculating the centers of mass of the refined light bulb regions within the original calibration images. However, due to measurement noise as well as eventual imperfections of the calibration board, in general, the estimated points do not correspond exactly to the calibration point positions in the real world coordinate system. In other words, there may not exist an homography which is able to map the coordinate points from the world coordinate system to the calibration image. A common solution to this problem is the use of the DLT algorithm [10] which results in a first approximation of the underlying homography. However, this approximation is not optimal since it is obtained by minimizing an algebraic distance measure which is not physically meaningful. Thus, we further refine the resultant homography by using the following cost function

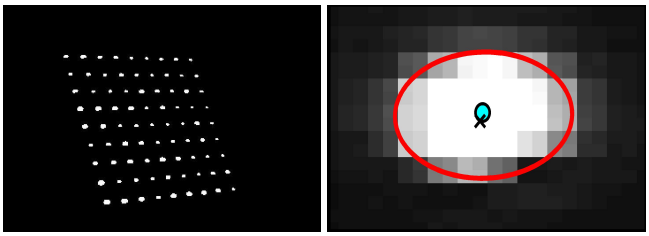

**Fig. 3:** *Results of the calibration point localization. (Left) Fig. 1 after application of the thresholding operation. (Right) Zoomed version of Fig. 1 showing a single light bulb region with superimposed ellipse, and the obtained calibration point before (circle) and after (cross) the minimization of eq. (5).*

$$\sum_i \left\| \mathbf{x}'_i - \mathbf{H}\bar{\mathbf{X}}'_i \right\|^2 , \tag{5}$$

where $\mathbf{x}'_i$ is the estimated position of the $i^{\text{th}}$ calibration point within the calibration image and $\bar{\mathbf{X}}'_i$ represents the position of the corresponding calibration point in the world coordinate system. The final, refined homography is the one for which the geometric error given by eq. (5) is minimized.

The final calibration point positions are computed by applying the refined homography to the calibration point positions in the world coordinate system. The right-hand side of Fig. 3 shows the resulting calibration point positions for a single light bulb region before and after minimizing the cost function of eq. (5).

### 3.2. Estimation of the IR camera parameters

Once the exact calibration point positions in each of the $N$ calibration images are known, the set of IR camera parameters can be estimated. This is accomplished by using a modified version of Zhang's algorithm [1] in which the tangential distortion of the employed lens is taken into consideration as well [14].

### 3.3. Iterative Calibration Point Refinement

A major limitation of most camera calibration approaches is that the actual calibration point localization is performed within non-fronto-parallel calibration images which suffer from nonlinear distortions due to the camera optics. In order to improve calibration results, it is therefore beneficial to first map the calibration images onto an undistorted fronto-parallel view (see left-hand side of Fig. 4) and determine the exact calibration point positions within these canonical images. However, in order to do so, full knowledge of the calibration parameters would be necessary - information that is usually not available. One possible solution to this problem was presented in [2] where the authors advocate an iterative refinement approach, using alternating mappings of the calibration images onto a canonical fronto-parallel view and back.

In this work we follow a similar approach. In more detail, we first remove the radial and tangential distortion from the calibration images, and map them onto a canonical fronto-parallel plane in the world coordinate system, using the previously calculated IR camera parameters. Within this fronto-parallel view we then localize the calibration points using the processing chain of Section 3.1. In a final

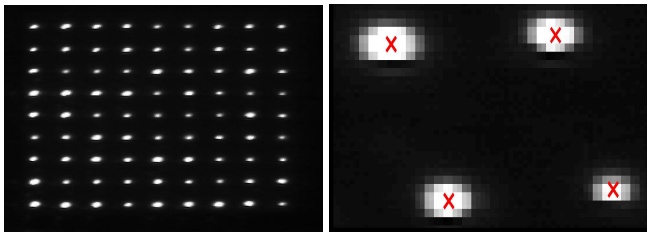

**Fig. 4:** *Results of the iterative calibration point refinement. (Left) Undistorted equivalent of Fig. 1 in the fronto-parallel plane. (Right) Final calibration point positions for a few selected light bulb regions.*

step, these new calibration points are remapped onto the original image plane and the IR camera parameters are recomputed using the updated calibration point positions. This process is repeated until convergence, where in each new loop the mapping onto the fronto-parallel plane is performed using the IR camera parameters from the previous iteration.

The left-hand side of Fig. 4 shows the undistorted equivalent of Fig. 1 in the fronto-parallel plane. A zoomed image with the resulting calibration point positions for a few selected light bulb regions after completion of the iterative refinement procedure is shown in the right-hand side of Fig. 4.

As it will be shown in the next section, the calibration parameters obtained by means of the refined calibration point positions result in a reprojection accuracy exceeding the one of traditional IR camera calibration approaches.

## 4. RESULTS

The proposed IR camera calibration scheme was applied to 18 views of the calibration board of Fig. 1, consisting of 81 light bulbs arranged in a $9 \times 9$ matrix. The distance between each of the light bulbs was 315 mm. The IR calibration images were obtained by grabbing selected frames of the analogue NTSC video output of a FLIR Prism DS camera, operating at a spectral range of 3.6 to 5 $\mu$m. Note that the actual camera calibration can be accomplished by means of a short video sequence, showing the rotational displacement of the calibration board. In order to convert the analogue video stream to digital data, a Blackmagic Decklink HD Extreme 3D video capturing card was utilized. In accordance with the NTSC standard, the resultant calibration images exhibit a resolution of $720 \times 486$ (which differs from the native resolution of the employed IR camera, $320 \times 244$). The lens distortion of the IR camera was assumed to comply with a $2^{\text{nd}}$ order radial distortion model with tangential distortion (see eq. (3)). The estimated set of intrinsic parameters measured in terms of pixels together with the corresponding standard deviations ($\sigma$) are given in Table 1.

In order to evaluate the accuracy of our calibration framework, we calculated the resulting mean reprojection error (MRE) when mapping the calibration point positions from the world coordinate system to the image plane, using the obtained set of calibration parameters. This is accomplished by computing the reprojection error of eq. (4) and averaging the result over all 18 views and 81 calibration points. Table 2 shows the resulting MRE of the proposed calibration scheme.

In order to assess the achieved result with the ones of the state-of-the-art, Table 2 also lists the MREs for some selected IR calibration schemes from the literature. Please note that these values were adapted to correspond to the image resolution of the IR calibration images used in this work. This normalization was deemed necessary since, as reported in Table 2, different camera models with differing image resolutions were employed in the quoted references.

| Parameters | Estimated values | $\sigma$ |
|---|---|---|
| $\alpha_x$ | 1868.3816 | 0.3902 |
| $\alpha_y$ | 1655.3959 | 0.3772 |
| $x_0$ | 312.4077 | 0.6621 |
| $y_0$ | 267.9757 | 0.5690 |
| $s$ | 0.0033 | 0 |
| $k_1$ | -0.5552 | 0.0012 |
| $p_1$ | -0.0069 | 0 |
| $p_2$ | 0.00572 | 0 |

**Table 1:** *Intrinsic calibration parameters of the IR camera.*

| Method | Camera | Resolution | MRE |
|---|---|---|---|
| Proposed | FLIR Prism DS | $720 \times 486$ | **0.0360** |
| Gschwandtner et al. [4] | PathfindIR | $360 \times 288$ | 0.4918 |
| Yang et al. [5] | GUIDE IR112 | $320 \times 240$ | 1.2214 |
| Vidas et al. [6] | Miricle 307K | $640 \times 480$ | 0.3031 |

**Table 2:** *MREs of the proposed IR camera calibration method and selected calibration schemes from the literature. The MREs of the quoted references were recomputed to fit the image resolution of the calibration images used in this work.*

At first glance it can be noticed that our method appears to improve the calibration results almost by a factor of 10 when compared to the state-of-the-art. However, it should be noted that due to possible differences in the simulation setup, a fair comparison cannot be conducted straightforwardly. Nevertheless, based on the vast differences between the MRE of the proposed scheme and the MREs of all remaining approaches, strong evidence exists that the proposed technique is indeed able to improve the accuracy of IR camera calibration distinctly.

IR cameras are often deployed together with visible-light cameras. Such multiple camera rigs are of special interest when a more elaborate description of the scene is necessary which cannot be provided by a single imaging sensor. Based on this observation, we additionally assessed our scheme when used to estimate the calibration parameters of a visible-light camera (Panasonic HDC-TM700). For this purpose, again, 18 images of the calibration device of Fig. 1 at a resolution of $640 \times 480$ were taken and the calibration parameters were calculated using the processing chain of Section 3. The attained MRE amounted to 0.0318 which is comparable to the results of other visible-light calibration schemes (see e.g. [2, 3]), indicating the suitability of the proposed algorithm for the calibration of cameras in both the IR and visible modality.

## 5. CONCLUSION

A novel iterative geometric IR camera calibration approach is presented in this work. Using a calibration board consisting of miniature light bulbs, our algorithm models the radiation pattern of each light bulb as an ellipse and regards the center of mass of the ellipsoidal region as the corresponding calibration point. In combination with an iterative refinement procedure, the localization accuracy of the calibration points is improved, resulting in a better estimate of the calibration parameters. We outlined the benefits of our solution by means of the reprojection error which was significantly reduced when compared to the state-of-the-art. Furthermore, we showed that the proposed scheme is also suitable for the calibration of visible-light cameras and thus can be employed for the calibration of multiple camera setups involving visible-light and IR cameras.

## 6. REFERENCES


[1] Z. Zhang, "A flexible new technique for camera calibration," *IEEE Transactions on Pattern Analysis and Machine Intelligence*, vol. 22, no. 11, pp. 1330 – 1334, November 2000.

[2] A. Datta, J.-S. Kim, and T. Kanade, "Accurate camera calibration using iterative refinement of control points," in *Proceedings of the 2009 IEEE International Conference on Computer Vision Workshops (ICCV Workshops)*, October 2009, pp. 1201 – 1208.

[3] C.D. Prakash and L.J. Karam, "Camera calibration using adaptive segmentation and ellipse fitting for localizing control points," in *Proceedings of the 2012 IEEE International Conference on Image Processing*, October 2012.

[4] M. Gschwandtner, R. Kwitt, A. Uhl, and W. Pree, "Infrared camera calibration for dense depth map construction," in *Proceedings of the 2011 Intelligent Vehicles Symposium*, June 2011, pp. 857 – 862.

[5] R. Yang, W. Yang, Y. Chen, and X. Wu, "Geometric calibration of IR camera using trinocular vision," *Journal of Lightwave Technology*, vol. 29, no. 24, pp. 3797 – 3803, December 2011.

[6] S. Vidas, R. Lakemond, S. Denman, C. Fookes, S. Sridharan, and T. Wark, "A mask-based approach for the geometric calibration of thermal-infrared cameras," *IEEE Transactions on Instrumentation and Measurement*, vol. 61, no. 6, pp. 1625 – 1635, June 2012.

[7] S. Lagüela, H. González-Jorge, J. Armesto, and P. Arias, "Calibration and verification of thermographic cameras for geometric measurements," *Infrared Physics & Technology*, vol. 54, no. 2, pp. 92 – 99, March 2011.

[8] A. Ellmauthaler, E.A.B. da Silva, C.L. Pagliari, and S.R. Neves, "Infrared-visible image fusion using the undecimated wavelet transform with spectral factorization and target extraction," in *Proceedings of the 2012 IEEE International Conference on Image Processing*, October 2012.

[9] A. Ellmauthaler, C.L. Pagliari, and E.A.B. da Silva, "Multiscale image fusion using the undecimated wavelet transform with spectral factorization and nonorthogonal filter banks," *IEEE Transactions on Image Processing*, vol. 22, no. 3, pp. 1005–1017, March 2013.

[10] R. Hartley and A. Zisserman, *Multiple View Geometry in Computer Vision*, Cambridge University Press, 2nd edition, 2004.

[11] J. Heikkilä and O. Silvén, "A four-step camera calibration procedure with implicit image correction," in *Proceedings of the 1997 IEEE Computer Society Conference on Computer Vision and Pattern Recognition*, June 1997, pp. 1106 – 1112.

[12] J. Heikkilä, "Geometric camera calibration using circular control points," *IEEE Transactions on Pattern Analysis and Machine Intelligence*, vol. 22, no. 10, pp. 1066 – 1077, October 2000.

[13] G. Bradski, A. Kaehler, and V. Pisarevsky, "Learning-based computer vision with intel's open source computer vision library," *Intel Technology Journal*, vol. 9, no. 2, pp. 119 – 130, May 2005.

[14] J.-Y. Bouguet, "Camera Calibration Toolbox for Matlab," http://www.vision.caltech.edu/bouguetj/calib_doc/, 2012, [Online; accessed 12/12/2012].

[15] S. Prakash, P.Y. Lee, T. Caelli, and T. Raupach, "Robust thermal camera calibration and 3D mapping of object surface temperatures," in *Proceedings of the XXVIII SPIE Conference on Thermosense*, 2006, vol. 6205.

[16] A. Yilmaz, K. Shafique, and M. Shah, "Target tracking in airborne forward looking infrared imagery," *Image and Vision Computing*, vol. 21, no. 7, pp. 623 – 635, 2003.

[17] T. Hastie, R. Tibshirani, and J. Friedman, *The Elements of Statistical Learning*, Springer Verlag, New York, 2nd edition, 2008.

[18] J. Canny, "A computational approach to edge detection," *IEEE Transactions on Pattern Analysis and Machine Intelligence*, vol. 8, no. 6, pp. 679 – 698, November 1986.

[19] A.W. Fitzgibbon, M. Pilu, and R.B. Fisher, "Direct least-squares fitting of ellipses," *IEEE Transactions on Pattern Analysis and Machine Intelligence*, vol. 21, no. 5, pp. 476 – 480, May 1999.